Proc. Natl. Acad. Sci. USA
Vol. 83, pp. 8589–8593, November 1986
Biophysics

Structural homology of reaction centers from *Rhodopseudomonas sphaeroides* and *Rhodopseudomonas viridis* as determined by x-ray diffraction

(bacterial photosynthesis/Patterson search method/membrane protein structure/structure of bacterial reaction centers)

J. P. ALLEN*, G. FEHER*, T. O. YEATES†, D. C. REES†, J. DEISENHOFER‡, H. MICHEL‡, AND R. HUBER‡

*University of California at San Diego, La Jolla, CA 92093; †University of California, Los Angeles, CA 90024; and ‡Max Planck Institute für Biochemie, D-8033 Martinsried/Munich, Federal Republic of Germany

Contributed by G. Feher, July 24, 1986

ABSTRACT **Crystals of the reaction center (RC) from *Rhodopseudomonas sphaeroides* with the space group $P2_12_12_1$, have been studied by x-ray diffraction. The Patterson search (molecular replacement) technique was used to analyze the data, with the structure of the reaction center from *Rhodopseudomonas viridis* as a model system. A preliminary electron density map of the reaction center from *R. sphaeroides* has been obtained. Comparison of the structure of the RC from *R. sphaeroides* with that from *R. viridis* showed the following conserved features: five membrane-spanning helices in each of the L and M subunits, a single membrane-spanning helix in the H subunit, a 2-fold symmetry axis, and similar positions and orientations of the cofactors. Unlike the RCs from *R. viridis*, both quinones are retained in the RCs from *R. sphaeroides*. The secondary quinone is located near the position related by the 2-fold symmetry axis to the primary quinone.**

Photosynthesis is the biological process by which light is converted into chemical energy. The primary photochemistry of light-induced electron transfer from a donor species to a series of acceptor species occurs in an integral membrane, pigment–protein complex called the reaction center (RC). The energy stored in the charge separation is supplied by light and used by the organism to drive electron-transfer reactions that are coupled to the synthesis of energy-rich compounds (e.g., ATP).

RCs from purple photosynthetic bacteria contain three subunits, L, M, and H (present in a 1:1:1 stoichiometry) and a number of cofactors: four bacteriochlorophylls (BChls), two bacteriopheophytins, two quinones, Q_A (primary electron acceptor), and Q_B (secondary electron acceptor), and one nonheme iron (for reviews, see refs. 1 and 2). Although RCs from different species exhibit many similarities in structure, there are some significant structural differences. The RCs from *Rhodopseudomonas sphaeroides* and *Rhodopseudomonas viridis* that are the subject of this investigation show the following differences. In *R. sphaeroides* the secondary, water-soluble cytochrome is not present in purified RCs. In contrast, RCs from *R. viridis* contain a fourth subunit, a cytochrome, that has four heme groups associated with it. The two species contain different types of BChl: *R. sphaeroides* has BChl-a whereas *R. viridis* contains BChl-b. The primary quinone in *R. sphaeroides* is a ubiquinone, whereas in *R. viridis* it is a menaquinone. Furthermore, the two quinones that serve as acceptors are retained in purified RCs from *R. sphaeroides*, but one is apparently lost from *R. viridis* during the purification.

Although extensive work has been done during the past two decades to characterize RCs, until recently there was very little information available on their three-dimensional structure. The reason was the lack of crystals suitable for x-ray diffraction studies. This situation changed with the successful crystallization of RCs from *R. viridis* (3) and *R. sphaeroides* (4, §). These crystals are of sufficient size and quality to obtain good x-ray diffraction data. The structure of the RCs from *R. viridis* has been reported recently at a resolution of 3 Å (5, 6).

In this work we describe the use of the Patterson search (molecular replacement) method (for reviews, see refs. 7 and 8) to obtain a low-resolution electron density map of the RC from *R. sphaeroides* and to show the homology between the structures of the RCs from the two bacterial species. A preliminary account of this work has been presented (9).

EXPERIMENTAL PROCEDURES

Crystallization. The RC from *R. sphaeroides* was crystallized by using the vapor diffusion technique. Different crystallization conditions produced a variety of forms as reported (4, 10, 11). The crystal form used for these structural studies was grown under the following conditions. The initial protein solution consisted of 5 mg of RC per ml, 0.36 M NaCl, 3.9% (wt/vol) heptane triol (mp, 80°C), 12% (wt/vol) PEG 4000, 0.06% lauryldimethylamine oxide, 15 mM Tris chloride (pH 8), 1 mM EDTA, and 0.1% NaN_3. This solution was equilibrated against 0.6 M NaCl/22% PEG 4000/15 mM Tris chloride/1 mM EDTA/0.1% NaN_3. After 3 weeks in the dark, crystals reached a typical size of 0.5 mm × 1 mm × 4–7 mm (Fig. 1). The space group has been identified as the orthorhombic form $P2_12_12_1$ with $a = 142.4$ Å, $b = 75.5$ Å, and $c = 141.8$ Å (11). The crystals have one RC per asymmetric unit and four RCs per unit cell; diffraction has been observed to a resolution of 3 Å.

Data Collection. Data were collected by using monochromator-filtered CuK_α radiation from an Elliot GX21 generator. X-ray intensity data were collected on a multiwire area detector of the type developed by Cork *et al.* (12). An initial 5-Å-resolution data set was collected from one crystal for the Patterson search study described in this paper. Algorithms for processing the detector images are described by Howard *et al.* (13). The ROCKS crystallographic computing system (14, 15) was used to scale and merge the data. No absorption corrections were applied. The R factor (defined as $R = \Sigma|I_i - I_j|/\Sigma|I_i + I_j|$, where the measured intensities I are summed over all symmetry-related reflections i and j) for merging this data set was 0.11.

The publication costs of this article were defrayed in part by page charge payment. This article must therefore be hereby marked "*advertisement*" in accordance with 18 U.S.C. §1734 solely to indicate this fact.

Abbreviations: RC, reaction center; BChl, bacteriochlorophyll; Q_A, primary quinone electron acceptor; Q_B, secondary quinone electron acceptor.

§Allen, J. P. & Feher, G., Meeting of the Biophysical Society, February 13–16, 1983, San Diego, CA.

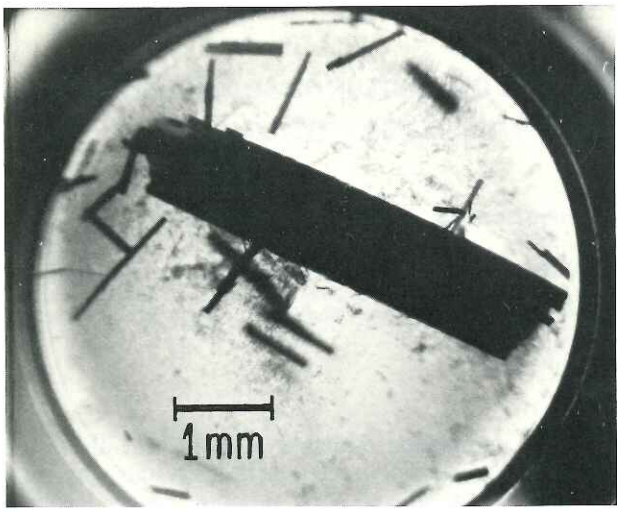

FIG. 1. RC crystals from *R. sphaeroides* (space group $P2_12_12_1$) grown by the vapor diffusion technique. For details see the text and refs. 10 and 11.

RESULTS AND DISCUSSION

The RC model used for the Patterson search work was constructed from a partially refined structure of the RC from *R. viridis*. The model contained all of the cofactors and the three subunits L, M, and H; the fourth nonconserved cytochrome subunit was removed. The conserved residues of L and M were retained, while all other residues, including all of H, were replaced by alanine. The 18 residues at the carboxyl terminus of the M subunit of the RC from *R. viridis* were removed because this polypeptide section is not present in the RCs from *R. sphaeroides*. Model structure factors were calculated with this model placed in a cubic cell (a = 160 Å) of $P1$ symmetry. The model was initially oriented with the 2-fold symmetry axis along z and the Fe at the origin (see Table 1).

The Patterson map for the model system was calculated between 25-Å and 5-Å resolution on a grid spacing of 1.67 Å. The Patterson map for the RC from *R. sphaeroides* data was calculated with the same resolution and grid. The rotation function was solved by using Patterson search methods and programs previously described (17). The 12,515 largest peaks in the model Patterson map within a radial shell of 20–45 Å were selected and rotated through a complete set of unique angles. For each orientation, the product correlation was calculated between the Patterson maps of the *R. viridis* model and the *R. sphaeroides* data set. The highest peak in the correlation function was 8 σ above the mean and 2 σ above the next highest peak. This orientation positions the 2-fold symmetry axis relating the L and M subunits near the diagonal of the crystallographic yz plane.

An independent test of the orientation of the RC from *R. sphaeroides* was obtained from a self-rotation function. A native Patterson map was calculated with data between 25 Å and 5 Å. The self-rotation function was calculated by rotating the highest 3818 peaks in this Patterson map (located in a radial shell between 5 Å and 30 Å about the origin) and comparing them to the unrotated Patterson map. This calculation showed a noncrystallographic 2-fold symmetry axis along the diagonal of the crystallographic yz plane (Fig. 2). This direction is consistent with the orientation of the local 2-fold axis of the RC as determined by the cross-rotation function.

The positioning of the correctly oriented model was achieved by using a translation function based upon the algorithm of Crowther and Blow (18). Intramolecular vectors were subtracted to enhance the signal-to-noise ratio of the map. Translation functions were calculated with the data from 25-Å to 5-Å resolution, as was used for the rotation function. In the space group $P2_12_12_1$, cross-vectors between symmetry-related molecules appear in the three Harker sections at $u = 1/2$, $v = 1/2$, and $w = 1/2$. For the correctly oriented model, the largest peak in each Harker section of the translation function corresponded to a single unique solution (Fig. 3).

Rigid-body refinement of the rotation and translation parameters (19) led to small shifts in these values. The parameters relating the crystallographic coordinate systems of the two species and the initial orientation of the model are given in Table 1. The R-factor between observed and calculated structure factors from the model was 0.43, for the data to 5-Å resolution.

A check of the crystal packing generated by the molecular replacement solution was satisfactory; there were no interpenetrations of molecules, and the lattice contact points all occurred in hydrophilic regions. This packing arrangement is similar to that observed in the structure of RCs from *R. viridis*.

The validity of the results of the Patterson search technique was confirmed with a set of higher-resolution (3.5-Å) data. Since the R factor, calculated with the 5-Å data, was only 0.43, substantial differences exist between the calculated structure and the true structure. To provide independent phasing information, we also used the isomorphous replacement technique. Both difference Patterson and difference Fourier calculations, using the model phases, indicate a consistent set of heavy-atom positions for a mercury derivative. Details of the higher resolution and isomorphous replacement results will be described in a later publication.

Comparison of the structure of the RC from *R. sphaeroides* with that from *R. viridis* showed many conserved features, such as the five membrane-spanning helices in each of the L and M subunits, the single membrane-spanning helix in the H subunit, and an approximate 2-fold symmetry axis between the L and M subunits. The positions and the orientations of the cofactors appear to be conserved, although slight differences between the two species cannot be ruled out at the present stage of analysis.

Table 1. Parameters relating the crystallographic coordinate systems of the RCs from *R. viridis* and *R. sphaeroides*

Transformation	Euler angles,* degrees	Translation vectors,* Å
R. viridis† → initial‡	325.0, 65.5, 152.5	26.9, 81.5, 125.0
Initial‡ → *R. sphaeroides*§	229.0, 142.0, 12.1	38.1, 29.8, 68.5
R. viridis† → *R. sphaeroides*§	119.8, 148.0, 153.1	−17.7, 147.1, −9.7

*Euler angles are in degrees as defined by Rossman and Blow (16). Translation vectors are in Angstroms along orthogonal x, y, and z axes, respectively.
†Coordinate system of the *R. viridis* RC in the unit cell of the *R. viridis* crystal.
‡Initial coordinate system of RC from *R. viridis* model with the local 2-fold along the z axis and the Fe at the origin.
§Coordinate system of the *R. viridis* RC in the unit cell of the *R. sphaeroides* crystal as determined by the Patterson search method.

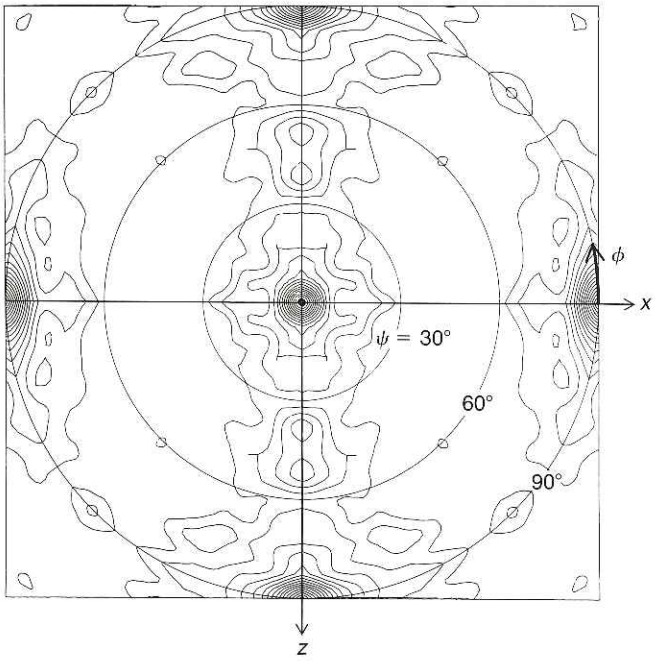

FIG. 2. Stereogram plot for 2-fold symmetry axes (κ = 180°) derived from correlation calculations in Patterson space using polar angles Ψ, the inclination against y, and the azimuth from the x axis, ϕ. Contour levels are from 2 σ above the average value in steps of 1 σ. The 2-fold axes along the x, y, and z axes are due to space group symmetry. The direction of the local 2-fold axis relating the L and M subunits is positioned near the diagonal of the yz plane.

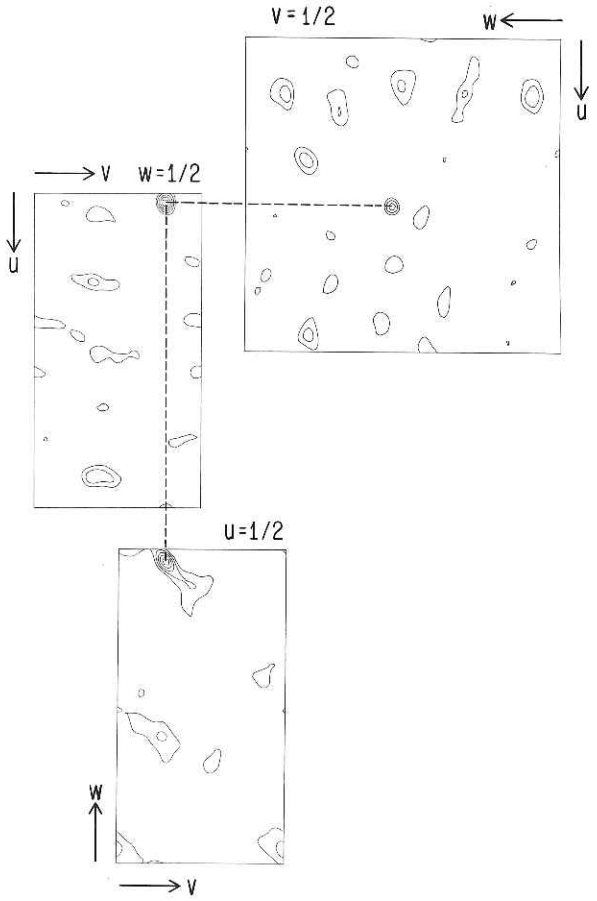

FIG. 3. Contour plots of the three Harker sections, located at u = 1/2, v = 1/2, and w = 1/2, for the translational function calculated with Patterson maps of the *R. viridis* model and the *R. sphaeroides* data. Contour levels are from 2 σ above the average value in steps of 1 σ. The largest peak in each Harker section (connected by the dashed line) corresponds to a single, unique solution (see Table 1).

The cofactor structures were examined against an electron density map generated by a difference Fourier calculation that provides an unbiased representation of the electron density. Specifically, the difference $(|F_0| - |F_c|)\exp(i\alpha_c)$ was calculated from the properly oriented model without the cofactors, where $|F_c|$ is the structure-factor amplitude and α_c is the calculated phase. Two specific regions, the primary donor (special BChl pair) and the secondary acceptor (ubiquinone-10), are illustrated in Fig. 4 *a* and *b*, respectively. These figures show sections of the difference maps calculated at 5-Å resolution with the positions of the cofactors superimposed. The cofactor positions were determined from the RC from the *R. viridis* model and have not been adjusted for optimal fit to the electron density.

Since Q_B is not present in the structure of the RC from *R. viridis*, its position was determined by rotating the primary acceptor Q_A (after replacing the second ring with two methoxy groups) about the 2-fold symmetry axis. The apparent shift from the calculated position to the position determined by the electron density map is either due to a difference in the local environment surrounding the Q_B binding site or due to a deviation from a strict 2-fold symmetry. The BChl dimer (Fig. 4*a*) corresponds well to the electron density map. The exact positions of the cofactors will be described after analysis of the higher resolution and isomorphous data is completed.

The homology between the two structures, in spite of the removal of the cytochrome subunit from the *R. viridis* model, suggests that there are no major structural changes associated with the binding of the cytochrome to the RC. Consequently, the difference in the binding strengths between the two species is most likely due to differences in the amino acid composition at the binding site or to the nonconserved M carboxyl terminus that is present near the cytochrome in the structure of the RC from *R. viridis* (6).

The structures of the RCs from *R. viridis* and *R. sphaeroides* confirm a number of structural features determined by spectroscopic and biochemical techniques. All of the cofactors are associated with the LM complex (1). The RC contains a BChl dimer that had been postulated to be the electron donor (20) and had been verified by electron paramagnetic resonance (EPR) and electron nuclear double resonance (ENDOR) experiments (21, 22). The structure contains a BChl and bacteriopheophytin monomer between the primary donor (BChl dimer) and primary acceptor (Q_A). This structure is consistent with the electron-transfer pathway as deduced from optical spectroscopy experiments (for reviews, see refs. 2, 23, and 24). Both quinones are present in the *R. sphaeroides* structure with the iron located between the two. The lack of an observed transmembrane potential associated with the electron transfer from Q_A^- to Q_B (25–27) suggested that the line joining the two quinones lies in the plane of the membrane; this is in agreement with the postulate that the 2-fold symmetry axis observed in the structure is perpendicular to the plane of the membrane (5, 6). That the iron is approximately equidistant from both quinones was suggested from an analysis of EPR data (28). The structure near the iron is in good agreement with the conclusions drawn from extended x-ray adsorption (EXAFS) studies (29, 30). A striking feature of the RC is the presence of the membrane-spanning helices. These had been predicted from an analysis of the hydropathy indices of the sequences of the subunits of RCs from *R. sphaeroides* (31, 32), *R. capsulata* (33), and *R. viridis* (34, 35).

The approximate 2-fold symmetry axis of the structure relates the L to the M subunit and the various cofactors (5, 6). This feature was surprising since one of the pathways is

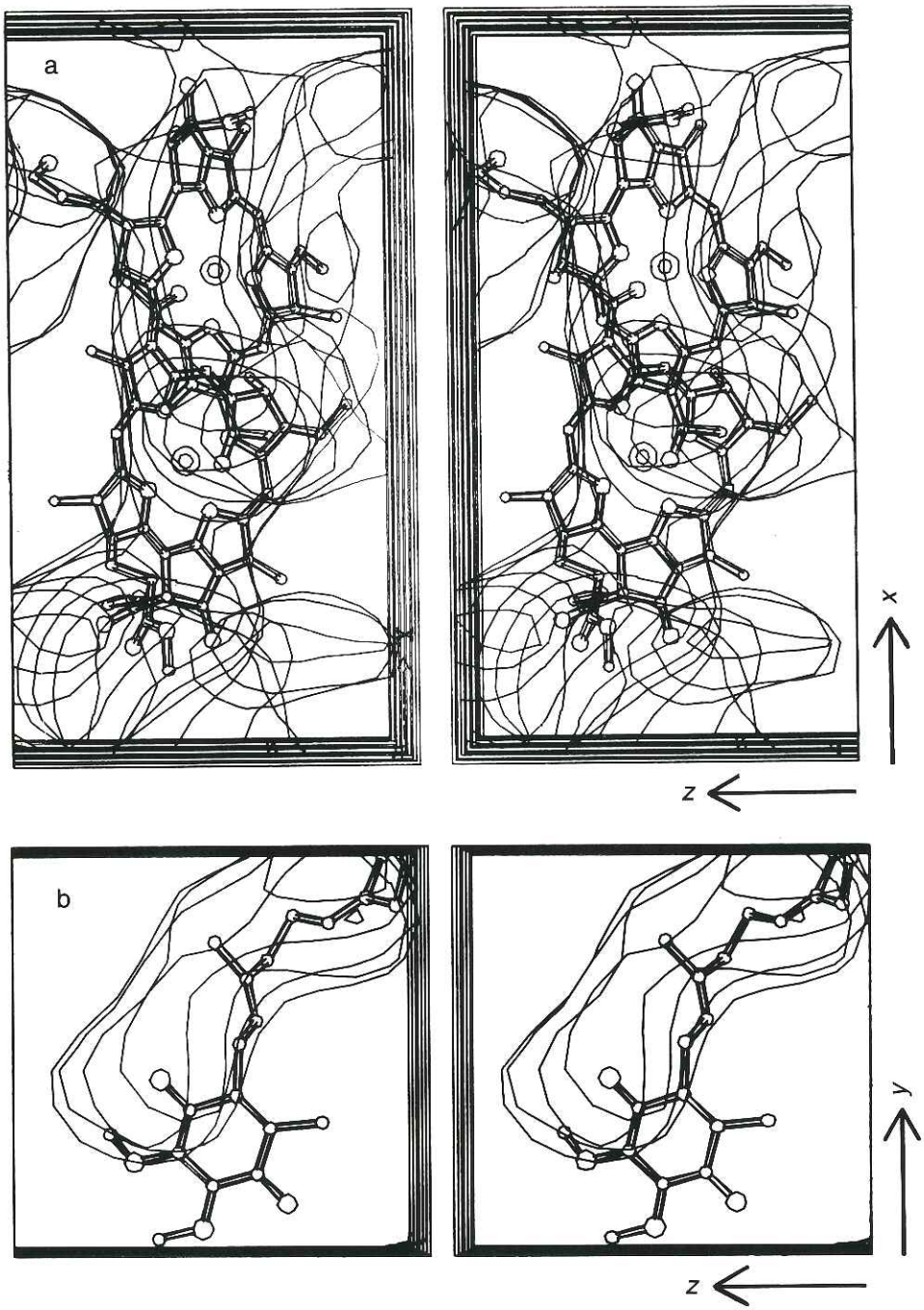

FIG. 4. Stereoplots of selected regions of a difference electron density map of the RC from *R. sphaeroides* at 5-Å resolution. Shown are the primary donor (*a*) and the second electron acceptor, Q_B (*b*). Each figure consists of contour plots of the electron density with the positions of the cofactors superimposed. The cofactor positions were determined from the RC from the *R. viridis* model and have not been adjusted for optimal fit to the electron density. For details of the calculation, see the text.

known to dominate the electron transfer. The 2-fold symmetry will undoubtedly be found to be broken by the protein environment. This should be revealed after the determination of the high-resolution structure has been completed.

Note Added in Proof. The positions and orientations of the cofactors and several amino acids of the RC from *R. sphaeroides* have been determined to a resolution of 3.3 Å. The data collection and analysis of the higher resolution data has been described (36). The RC model was refined by using the restrained least-squares program of Hendrickson and Konnert as in ref. 37. At the present stage of refinement, the *R* factor between observed and calculated structure factors is 0.306 for data between 8-Å and 3.3-Å resolution, with the deviation of bond distances from standard values being 0.023 Å. The structure of the primary donor is shown in Fig. 5*a*. The angle between the normals of the planes of the two BChl rings is ≈10°, and the angle between the lines connecting the nitrogens of pyrrole rings I and III is ≈140°. For the two BChls, the separation between the planes of rings I is ≈3.5 Å, and the separation of the Mg atoms is ≈7.5 Å. The structure of the secondary electron acceptor, Q_B, the nearby amino acids, and the position of the Fe are shown in Fig. 5*b*. The structure indicates that the oxygens of Q_B are hydrogen bonded to His-190 of subunit L (His-L190) and to Ser-L223. His-L190 is also liganded to the iron, as shown in Fig. 5*b*. Mutations in either Ile-L229 or Ser-L223 in RCs from *R. sphaeroides* have been found to alter the binding of Q_B and to impart herbicide resistance to the bacteria (38). Although the cofactors follow the 2-fold symmetry in general, the average position of the ring atoms of Q_B deviates by ≈2 Å from those obtained by rotating the atoms of Q_A around the 2-fold axis. Chang *et al.* recently reported x-ray diffraction results on crystals of RCs from *R. sphaeroides* (39). Their results confirm our previous findings that the structure of the RC from *R. sphaeroides* is very homologous to that of *R. viridis* (4).

We thank E. Abresch for the preparation of the RCs and H. Komiya for assistance with the data analysis. This work was supported by grants from the National Institutes of Health (AM36053, GM13191, and GM31875) and the Chicago Community Trust/Searle Scholars Program.

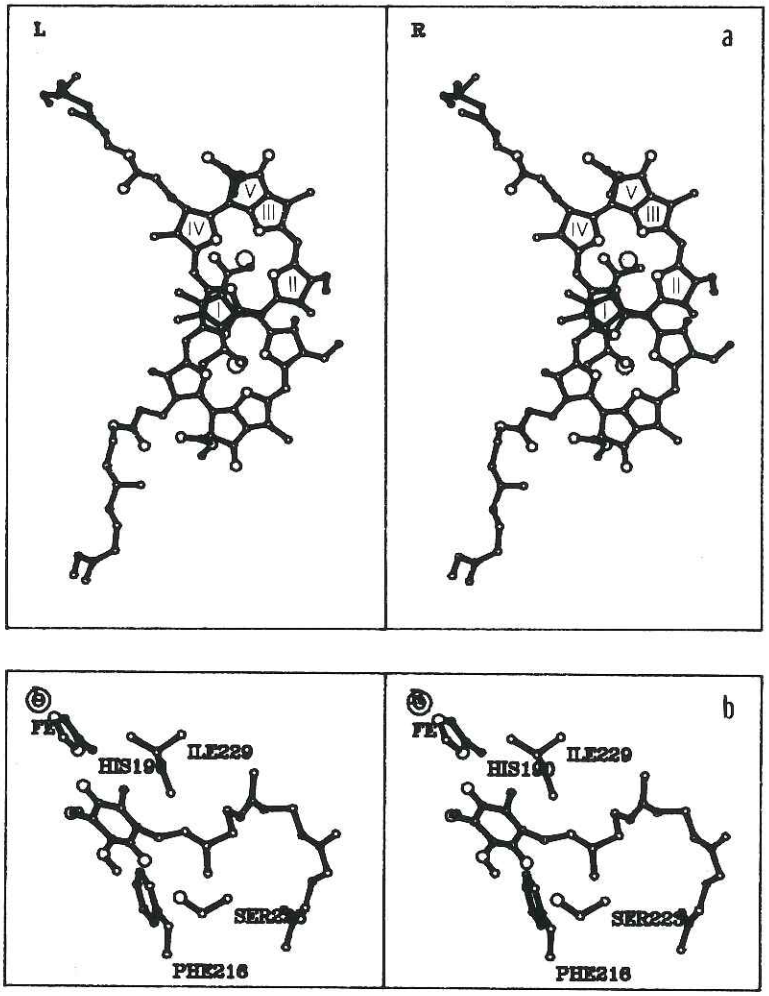

FIG. 5. Stereoplots of the primary donor (*a*) and the secondary electron acceptor, Q_B, the nearby amino acids, and the Fe (*b*) at 3.3 Å resolution.

1. Feher, G. & Okamura, M. Y. (1978) in *The Photosynthetic Bacteria*, eds. Clayton, R. K. & Sistrom, W. R. (Plenum, New York), pp. 349–386.
2. Okamura, M. Y., Feher, G. & Nelson, N. (1982) in *Photosynthesis*, ed. Govindjee (Academic, New York), pp. 195–272.
3. Michel, H. (1982) *J. Mol. Biol.* **158,** 567–572.
4. Allen, J. P. & Feher, G. (1984) *Biophys. J.* **45,** 256a (abstr.).
5. Deisenhofer, J., Epp, O., Miki, K., Huber, R. & Michel, H. (1984) *J. Mol. Biol.* **180,** 385–398.
6. Deisenhofer, J., Epp, O., Miki, K., Huber, R. & Michel, H. (1985) *Nature (London)* **318,** 618–624.
7. Rossman, M. G., ed. (1972) in *The Molecular Replacement Method* (Gordon & Breach, New York).
8. Huber, R. (1969) in *Crystallographic Computing*, ed. Ahmed, F. R. (Munksgaard, Copenhagen), pp. 96–102.
9. Allen, J. P., Feher, G., Yeates, T. O., Rees, D. C., Eisenberg, D. S., Deisenhofer, J., Michel, H. & Huber, R. (1986) *Biophys. J.* **49,** 583a (abstr.).
10. Allen, J. P. & Feher, G. (1984) *Proc. Natl. Acad. Sci. USA* **81,** 4795–4799.
11. Feher, G. & Allen, J. (1985) in *Molecular Biology of the Photosynthetic Apparatus* (Cold Spring Harbor Laboratory, Cold Spring Harbor, NY), pp. 163–172.
12. Cork, C., Hamlin, R., Vernon, W., Xuong, N. H. & Perez-Mendez, V. (1975) *Acta Crystallogr. Sect. A* **31,** 702–703.
13. Howard, A. J., Nielsen, C. & Xuong, N. H. (1985) *Methods Enzymol.* **114,** 452–472.
14. Reeke, G. N. (1984) *J. Appl. Crystallogr.* **17,** 125–130.
15. Bethge, P. H. (1984) *J. Appl. Crystallogr.* **17,** 215.
16. Rossmann, M. G. & Blow, D. M. (1962) *Acta Crystallogr.* **15,** 24–31.
17. Huber, R. (1965) *Acta Crystallogr.* **19,** 353–356.
18. Crowther, R. A. & Blow, D. M. (1967) *Acta Crystallogr.* **23,** 544–548.
19. Huber, R. & Schneider, M. (1985) *J. Appl. Crystallogr.* **18,** 165–169.
20. Norris, J. R., Druyan, M. E. & Katz, J. J. (1973) *J. Am. Chem. Soc.* **95,** 1680–1682.
21. Feher, G., Hoff, A. J., Isaacson, R. A. & Ackerson, L. C. (1975) *Ann. N.Y. Acad. Sci.* **244,** 239–259.
22. Norris, J. R., Scheer, H. & Katz, J. J. (1975) *Ann. N.Y. Acad. Sci.* **244,** 261–280.
23. Cramer, W. A. & Crofts, A. R. (1982) in *Photosynthesis*, ed. Govindjee (Academic, New York), pp. 387–467.
24. Parson, W. W. & Ke, B. (1982) in *Photosynthesis*, ed. Govindjee (Academic, New York) pp. 331–385.
25. Packham, N. K., Dutton, P. L. & Mueller, P. (1982) *Biophys. J.* **37,** 465–473.
26. Blatt, Y., Gopher, A., Montal, M. & Feher, G. (1983) *Biophys. J.* **41,** 121a (abstr.).
27. Feher, G. & Okamura, M. Y. (1984) in *Advances in Photosynthesis Research*, ed. Sybesma, C. (M. Nijhoff/W. Junk, Publishers, Brussels), pp. 155–164.
28. Butler, W. F., Calvo, R., Fredkin, D. R., Isaacson, R. A., Okamura, M. Y. & Feher, G. (1984) *Biophys. J.* **45,** 947–973.
29. Eisenberger, P., Okamura, M. Y. & Feher, G. (1982) *Biophys. J.* **37,** 523–538.
30. Bunker, G., Stern, E. A., Blankenship, R. E. & Parson, W. W. (1982) *Biophys. J.* **37,** 539–551.
31. Williams, J. C., Steiner, L. A., Ogden, R. C., Simon, M. I. & Feher, G. (1983) *Proc. Natl. Acad. Sci. USA* **80,** 6505–6509.
32. Williams, J. C., Steiner, L. A., Feher, G. & Simon, M. I. (1984) *Proc. Natl. Acad. Sci. USA* **81,** 7303–7307.
33. Youvan, D. C., Bylina, E. J., Alberti, M., Begusch, H. & Hearst, J. E. (1984) *Cell* **37,** 949–957.
34. Michel, H., Weyer, K. A., Gruenberg, H. & Lottspeich, F. (1985) *EMBO J.* **4,** 1667–1672.
35. Michel, H., Weyer, K. A., Gruenberg, H., Dunger, I., Oesterhelt, D. & Lottspeich, F. (1986) *EMBO J.* **5,** 1149–1158.
36. Allen, J. P., Feher, G., Yeates, T. O. & Rees, D. C. (1986) in *Proceedings of the Seventh International Congress on Photosynthesis* (Nijhoff/Junk, Brussels, Belgium), in press.
37. Hendrickson, W. A. (1985) *Methods Enzymol.* **115,** 252–270.
38. Paddock, M. L., Williams, J. C., Rongey, S. H., Abresch, E. C., Feher, G. & Okamura, M. Y. (1986) in *Proceedings of the Seventh International Congress on Photosynthesis* (Nijhoff/Junk, Brussels, Belgium), in press.
39. Chang, C. H., Tiede, D., Tang, J., Smith, U., Norris, J. & Schiffer, M. (1986) *FEBS Lett.* **205,** 82–86.